Acknowledgment. We are grateful to the donors of the Petroleum Research Fund, administered by the American Chemical Society, for support of this research and to Jonathan Pope for his help with the research. The purchase of the diffractometer was supported in part by NSF Grant CHE 8000670.

Registry No. $[Co(18S6)](picrate)_2$, 33270-89-2; $[Co(2,5,8\text{-trithianonane})_2](BF_4)_2$, 99797-09-8.

Supplementary Material Available: Listings of anisotropic thermal parameters, hydrogen atom positional and thermal parameters, interatomic distances and angles, and observed and calculated structure factors (41 pages). Ordering information is given on any current masthead page.

Chiroptical Properties of Compounds Containing Metal–Metal Bonds. Syntheses, Structures, and the Measurement and Interpretation of Electronic and Circular Dichroism Spectra of $Rh_2[(S)\text{-mandelate}]_4(EtOH)_2$ and $Rh_2[(R)\text{-}\alpha\text{-methoxy-}\alpha\text{-phenylacetate}]_4(THF)_2$

Pradyot A. Agaskar, F. Albert Cotton,* Larry R. Falvello,* and Scott Han

Contribution from the Department of Chemistry and Laboratory for Molecular Structure and Bonding, Texas A&M University, College Station, Texas 77843. *Received July 29, 1985*

Abstract: The preparation, the electronic and circular dichroism spectra in solution, and the crystal and molecular structures of two chiral dirhodium tetracarboxylato complexes are reported. $Rh_2[(S)\text{-mandelate}]_4(EtOH)_2$ (**1**) was prepared by reaction of $RhCl_3\cdot 3H_2O$ and (*S*)-mandelic acid (α-hydroxy-α-phenylacetic acid) in aqueous solution in the presence of dimethylformamide, followed by recrystallization from ethanol. Compound **1** crystallizes in the orthorhombic space group $P2_12_12_1$ with a = 9.027 (2) Å, b = 27.110 (5) Å, c = 32.656 (5) Å, V = 7991 (4) Å^3, and Z = 8. The structure was refined to least-squares residuals of R = 0.0455, R_w = 0.0551, and quality-of-fit = 1.026. $Rh_2[(R)\text{-}\alpha\text{-methoxy-}\alpha\text{-phenylacetate}]_4(THF)_2$ (**2**), prepared by reaction of $RhCl_3\cdot 3H_2O$ with (*R*)-α-methoxy-α-phenylacetic acid in water/ethanol, followed by extraction with THF, crystallizes in the triclinic space group $P\bar{1}$ with a = 11.263 (2) Å, b = 20.544 (3) Å, c = 10.325 (2) Å, α = 91.83 (1)°, β = 110.21 (1)°, γ = 89.11 (1)°, V = 2234.5 (6) Å^3, and Z = 2. The structure was refined to least-squares residuals of R = 0.0460, R_w = 0.0543, and quality-of-fit = 1.004. Absolute configurations were determined for both structures. The electronic spectra of **1** and **2** have bands near 600 and 450 nm in the visible region. The circular dichroism spectrum of each compound has three prominent bands, two bands with the same sign near 600 and 450 nm and a third band at 500 nm, opposite in sign to the first two. The circular dichroism effects are interpreted in terms of a static-coupling mechanism. The bands at 600 and 400 nm are assigned as electronically allowed components of the transitions π^*(Rh–Rh) → σ^*(Rh–O) and π(Rh–Rh, Rh–O) → σ^*(Rh–O), respectively. The band at 500 nm is assigned as an overlap of magnetically allowed components of the same transitions.

Over the past two decades a substantial body of literature has described the preparation and structures of the metal–metal singly bonded dirhodium complexes, the most common of which are the tetracarboxylato compounds of the type $Rh_2(O_2CR)_4L_2$, in which L represents a Lewis base and R an organic group.[1] Following an early report of a preparation[2] and the first accurate structure determination,[3] some three score compounds have been prepared and structurally characterized.[4]

In marked contrast to the large body of accurate structural characterization, the description of the electronic structures of these compounds has presented a more difficult problem. The electronic spectra show two predominant peaks in the visible region. The higher energy transition, which typically appears at ~450 nm and is often a shoulder on a charge-transfer band, is relatively insensitive to the nature of the axial ligand, while the lower energy band varies in the range 500–600 nm, depending on the identity of the axial donor atom. For complexes with oxygen donor atoms in the axial positions, the lower energy band appears at or near 600 nm.

Single-crystal electronic spectra were first reported by Martin and co-workers,[5] who measured the spectrum of a monoclinic crystal of $Rh_2(O_2CCH_3)_4(H_2O)_2$ at both 300 and 15 K. The low-energy band was found to be polarized perpendicular to the metal–metal bond, while the higher energy band was found to consist of two transitions, one polarized parallel to and one perpendicular to the crystallographic *b*-axis. All of the evidence at this point appeared consistent with an earlier assignment, based on Xα calculations,[6] which attributed the lower energy band to the transition π^*(Rh–Rh) → σ^*(Rh–Rh) ($^1A_{1g} \rightarrow {}^1E_u$ in D_{4h} symmetry). The (*xy*) component of the higher energy band (450 nm) was assigned to the transition π^*(Rh–Rh) → σ^*(Rh–O) (also $^1A_{1g} \rightarrow {}^1E_u$).

While these assignments were fully in line with the energies of the observed electronic transitions, a question remained about the Rh–Rh vibrational stretching frequency. Martin et al. observed a vibrational progression, with an average splitting of 297 cm^{-1}, on the 600-nm band at 15 K, implying a metal–metal stretching frequency of 297 cm^{-1} for the excited state. While ν(Rh–Rh) values in the range of 288–351 cm^{-1} have been suggested,[7,8] these values are quite high for a stretch involving singly

(1) Cotton, F. A.; Walton, R. A. "Multiple Bonds Between Metal Atoms"; Wiley: New York, 1982.
(2) Chernyaev, I. I.; Shenderetskaya, E. V.; Koryagina, A. A. *Russ. J. Inorg. Chem.* (*Engl. Transl.*) **1960**, *5*, 559.
(3) Cotton, F. A.; DeBoer, B. G.; LaPrade, M. D.; Pipal, J. R.; Ucko, D. A. *J. Am. Chem. Soc.* **1970**, *92*, 2926. Cotton, F. A.; DeBoer, B. G.; LaPrade, M. D.; Pipal, J. R.; Ucko, D. A. *Acta Crystallogr., Sect. B: Struct. Crystallogr. Cryst. Chem.* **1971**, *B27*, 1664.
(4) Felthouse, T. R. *Prog. Inorg. Chem.* **1982**, *29*, 73.
(5) Martin, D. S.; Webb, T. R.; Robbins, G. A.; Fanwick, P. E. *Inorg. Chem.* **1979**, *18*, 475.
(6) Norman, J. G.; Kolari, H. J. *J. Am. Chem. Soc.* **1978**, *100*, 791.
(7) Ketteringham, A. P.; Oldham, C. *J. Chem. Soc., Dalton Trans.* **1973**, 1067.
(8) Moller, M. R.; Bruck, M. A.; O'Connor, T.; Armatis, F. J.; Knolinski, E. A.; Kottmair, N.; Tobias, R. S. *J. Am. Chem. Soc.* **1980**, *102*, 4589.

0002-7863/86/1508-1214$01.50/0

bonded rhodium atoms. Raman experiments[9-11] and normal-coordinate analysis[12] have led some workers to suggest a value of ca. 170 cm^{-1} for ν(Rh–Rh).

Recently, Gray et al. have reassigned the transitions observed in the electronic spectra of singly bonded dirhodium complexes.[13] The (x,y)-polarized band at ~600 nm has been attributed to the transition π^*(Rh–Rh) → σ^*(Rh–O), while the (x,y)-polarized band at ~450 nm has been assigned to π(Rh–Rh,Rh–O) → σ^*(Rh–O). Gray et al. measured single-crystal spectra from tetragonal crystals of $Li_2Rh_2(O_2CCH_3)_4Cl_2 \cdot 8H_2O$, which had the advantageous property of allowing direct measurement of the polarized molecular spectra from the crystals. The new assignments are fully consistent with all experimental and theoretical data. Furthermore, the vibrational progression on the ~600-nm band can now be attributed to the symmetrical Rh–O(carboxylate) stretch, which is a more acceptable assignment for the observed splitting of 297 cm^{-1} than is ν(Rh–Rh).

It is well-known that when a chromophore can be placed in a chiral environment, chiroptical properties (ORD, CD) will become manifest and that these properties will be a sensitive function of the electronic character of the ground and excited states of the system. The measurement of these chiroptic properties affords a rich source of useful and cogent data with which to establish the correct assignments of electronic transitions.

We report here the results of our studies of the chiroptical properties of two new, chiral complexes containing singly bonded dirhodium cores. While supporting the recent assignment of the electronic spectrum by Gray et al., our results shed new light on the electronic structure of the Rh_2^{4+} chromophore. We have observed (vide infra) a previously unseen, magnetically allowed transition at 500 nm in the circular dichroism spectra of the two complexes, $Rh_2((S)\text{-mand})_4(EtOH)_2$ (**1**) (mand = mandelate, α-hydroxy-α-phenylacetate), and $Rh_2((R)\text{-mpa})_4(THF)_2$ (**2**) (mpa = α-methoxy-α-phenylacetate). We interpret the results in terms of a static coupling mechanism between the achiral chromophore and its chiral surroundings.

Chiroptical properties of in situ complexes containing metal–metal bonds have been explored by Snatzke[14,15] as a means of determining the absolute configurations of organic ligands. In the present work we have used ligands of known stereochemistry as a means of elucidating the electronic structure of the inorganic chromophore.

Experimental Section

Preparation of $Rh_2[(S)\text{-mandelate}]_4(EtOH)_2$ (1). In an open beaker, 0.5 g (1.9 mmol) of $RhCl_3 \cdot 3H_2O$ was dissolved in 6 mL of distilled water. To this solution was added 5 mL of a saturated aqueous solution of (*S*)-mandelic acid and 0.5 mL of dimethylformamide. This mixture was heated on a water bath at 80 °C for 6 h, while the solution level was maintained by regular additions of distilled water. At the end of the 6 h of heating, the blue-green precipitate which had formed was filtered and washed with water. The product was dried in vacuo at 100 °C for 1 h. The yield of dried product was 42%, based on $RhCl_3 \cdot 3H_2O$. A similar procedure using the enantiomeric (*R*)-mandelic acid gave a yield of 38%. The compound is soluble in ethanol and acetone, but it is insoluble in water. Crystals suitable for X-ray diffraction were grown by slow evaporation of an ethanol solution in air.

Preparation of $Rh_2[(R)\text{-}\alpha\text{-methoxy-}\alpha\text{-phenylacetate}]_4(THF)_2$ (2). A mixture of 0.10 g (0.38 mmol) of $RhCl_3 \cdot 3H_2O$ and 0.13 g (0.76 mmol) of (*R*)-α-methoxy-α-phenylacetic acid dissolved in 15 mL of 1:1 H_2O/EtOH was heated at reflux for 1 h. The resulting mixture contained both rhodium metal and a blue-green precipitate of the desired product. After cooling, the solid was filtered; and the blue-green product was extracted with 40 mL of tetrahydrofuran. The extract was filtered, and the filtrate was evaporated. The resulting solid was dried for 30 min in vacuo at 80 °C. The yield was 33%, based on $RhCl_3 \cdot 3H_2O$. Crystals suitable for X-ray analysis were grown by slow evaporation of a THF solution of the product.

Spectroscopic Measurements. The UV/vis spectra of compounds **1** and **2** in ethanol and THF, respectively, were taken at ambient temperature, on a Cary 17-D spectrophotometer. Qualitative circular dichroism spectra were taken from the same solutions, on a Cary 60 spectropolarimeter. The solutions were prepared by dissolving a portion of the crystals prepared for X-ray diffraction (as described above) in the appropriate solvent.

X-ray Data Collection, Structure Solution, and Refinement. Crystals of **1** and **2** were mounted at the ends of glass fibers. Data were gathered by routine procedures described previously.[16] The data collection and crystal parameters are summarized in Table I. For both compounds, the data were reduced by routine procedures,[17] including the application of an empirical absorption correction[18] based on azimuthal scans of several reflections with diffractometer angle χ near 90°.

Crystals of both compounds were found to have two molecules in the asymmetric unit. For compound **1** (space group $P2_12_12_1$) the positions of the four independent rhodium atoms were found by direct methods. The structure was developed and refined in an alternating sequence of least-squares refinements and difference maps. The final full-matrix least-squares cycle for the correct enantiomorph (vide infra) fitted 939 parameters to 5890 unique data with $F_o^2 > 3\sigma(F_o^2)$. Each Friedel pair was treated as two separate data. In the final refinement two atoms, O(11) and C(18), were refined isotropically, since their anisotropic thermal parameters from previous refinements were not positive-definite. In addition, a lattice ethanol molecule was assigned a fixed multiplicity of 0.85. This value had been established in an earlier refinement in which the multiplicity of this group had been refined. The final cycle did not shift any parameter by more than 0.20 times its standard deviation. The least-squares residuals from the last cycle (Table I) are $R = 0.0455$ and $R_w = 0.0551$.

For compound **2**, the positions of the four unique rhodium atoms were derived from the Patterson map. The remaining non-hydrogen atoms were located and refined in a series of least-squares refinements and difference maps. In the final full-matrix least-squares cycle, 1078 parameters for 120 atoms (all anisotropic) were refined to 6516 unique data with $F_o^2 \geq 3\sigma(F_o^2)$. As before, each Friedel pair present in the data was treated as two distinct observations. The final cycle, which did not shift any parameter by more than 0.27 times its estimated standard deviation, gave residuals of $R = 0.0460$ and $R_w = 0.0543$ (Table I).

Determination of Absolute Configurations from X-ray Data. Each of the compounds was refined to convergence in both enantiomorphs, by full-matrix weighted least-squares analysis. The correct enantiomorph in each case was established by application of the Hamilton significance test.[19]

For compound **1**, the (*S*)-configuration of the bridging mandelate ligands was established at the 99% confidence level. The (*S*)-enantiomer gave a weighted *R*-factor of 0.0551, while the (*R*)-enantiomer gave $R_w = 0.0568$. A comparison of the ratio $R_w(R)/R_w(S)$ (= 1.030) to the significance point $R_{1,4951,0.01}$ (calculated as 1.006 according to Hamilton[19,20]) established the presence of the (*S*)-configuration.

For compound **2**, the weighted *R*-factors for the (*R*)- and (*S*)-enantiomers were 0.0543 and 0.0557, respectively, giving $R_w(S)/R_w(R) = 1.026$. Comparison of this value with the significance point[20] $R_{1,5438,0.01}$ (1.006) established the presence of the (*R*)-configuration at the 99% confidence level.

(9) Kharitonov, Y. Y.; Mazo, G. Y.; Knyazeva, N. A. *Russ. J. Inorg. Chem.* **1970**, *15*, 739.
(10) San Filippo, J.; Sniadoch, H. *Inorg. Chem.* **1973**, *12*, 2326.
(11) Baranovskii, I. B.; Golubnichaya, M. A.; Mazo, G. Y.; Nefedov, V. I.; Salyn, Y. V.; Shchelokov, R. N. *Russ. J. Inorg. Chem.* **1976**, *21*, 591.
(12) Kireeva, I. K.; Mazo, G. Y.; Shchelokov, R. N. *Russ. J. Inorg. Chem.* **1979**, *24*, 220.
(13) Miskowski, V. M.; Schaefer, W. P.; Sadeghi, B.; Santarsiero, B. D.; Gray, H. B. *Inorg. Chem.* **1984**, *23*, 1154.
(14) Snatzke, G. *Angew. Chem., Int. Ed. Engl.* **1979**, *18*, 363.
(15) Frelek, J.; Perkowska, A.; Snatzke, G.; Tima, M.; Wagner, U.; Wolff, H. P. *Spectrosc. Int. J.* **1983**, *2*, 274.
(16) (a) Bino, A.; Cotton, F. A.; Fanwick, P. E. *Inorg. Chem.* **1979**, *18*, 3558. (b) Cotton, F. A.; Frenz, B. A.; Deganello, G.; Shaver, A. *J. Organomet. Chem.* **1973**, *50*, 227.
(17) Crystallographic calculations were done on a VAX-11/780 (VMS V3.6) computer with software from the package VAXSDP and on a PDP-11/60 (RSX-11M V4.1) with software from SDP-PLUS.
(18) North, A. C. T.; Phillips, D. C.; Mathews, F. S. *Acta Crystallogr. Sect. A: Cryst. Phys., Diffr., Theor. Crystallogr.* **1968**, *24*, 351.
(19) Hamilton, W. C. *Acta Crystallogr.* **1965**, *18*, 502.
(20) The significance points were calculated from Hamilton's formula:

$$R_{b,n-m,\alpha} = \left(\frac{b}{n-m} F_{b,n-m,\alpha} + 1\right)^{1/2}$$

in which b is the dimension of the hypothesis ($b = 1$ for a change of enantiomorph); $(n - m)$ is the number of degrees of freedom ($n - m = 4951$ and 5438 for compounds **1** and **2**, respectively); α is the significance level; and $F_{b,n-m,\alpha}$ is a statistical analysis-of-variance ratio, obtained by harmonic interpolation of values in a standard compilation: Keeping, E. S. "Introduction to Statistical Inference"; Van Nostrand: Princeton, NJ, 1962.

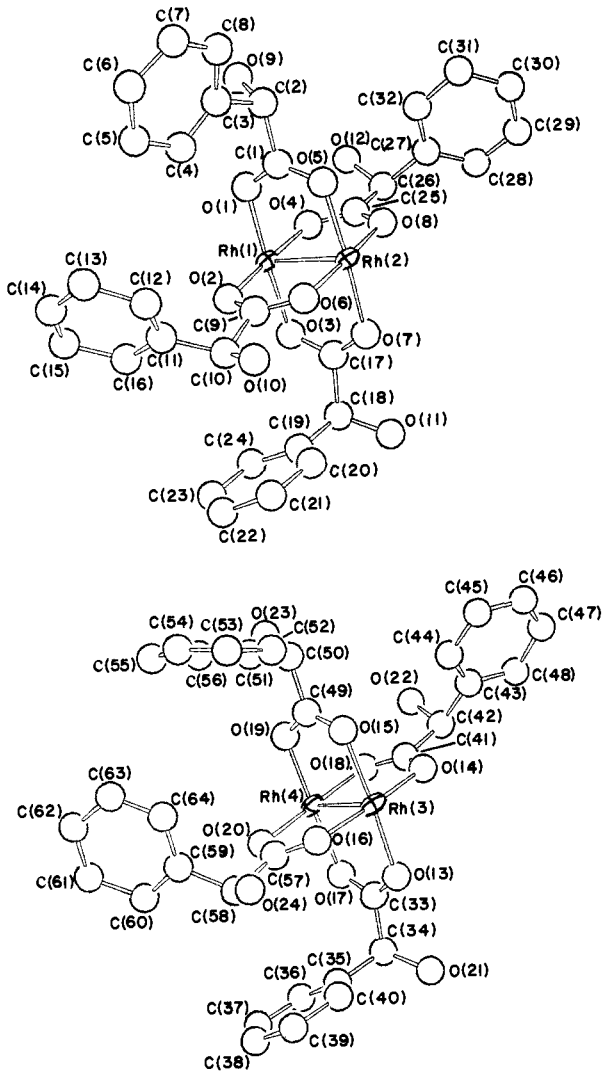

Figure 1. (a) Molecule 1 and (b) molecule 2 from the crystal structure of $Rh_2((S)$-mandelate$)_4(EtOH)_2 \cdot 0.43EtOH$, **1**. The atom labeling scheme is shown. Axial ethanol moieties have been omitted for clarity.

Results and Discussion

Crystal Structures of $Rh_2((S)$-mand$)_4(EtOH)_2 \cdot 0.43EtOH$ (1) and $Rh_2((R)$-mpa$)_4(THF)_2$ (2). Compounds **1** and **2** both have the same coordination geometry observed in all of the previously characterized singly bonded dirhodium tetracarboxylates, with local D_{4h} symmetry at the $Rh_2(O_{eq})_8(O_{ax})_2$ chromophore. (The symmetry is reduced to D_{2h} in each case if the anisotropy of the full axial ligand is considered and to C_1 for the entire molecule.) Both compounds crystallize with two independent molecules in the asymmetric unit. Figure 1 shows the structure and labeling scheme for each of the molecules in the structure of **1**, and Figure 2 shows the molecules from the structure of **2**. Tables II and III give the atomic coordinates and equivalent isotropic thermal parameters for **1** and **2**, respectively. Selected bond lengths and angles for compounds **1** and **2** are given in Tables IV and V, respectively; and average distances and angles for both structures are listed in Table VI. The Rh–Rh bond lengths from the two structures (**1**: 2.386 (2) and 2.386 (2) Å; **2**: 2.391 (1), 2.389 (1) Å) are almost identical and are within the narrow range of distances observed in previously characterized singly bonded rhodium dimers.[1] The coordination geometry about the rhodium centers also gives no surprises. (See Tabel VI.) The absolute configurations at the α-carbon atoms can be clearly seen in Figures 1 and 2.

For the structure of **1**, we found it particularly desirable to establish the absolute configuration crystallographically, since the starting material was labeled "*d*-mandelic acid"; and we as yet know of no previous work from outside this laboratory which has

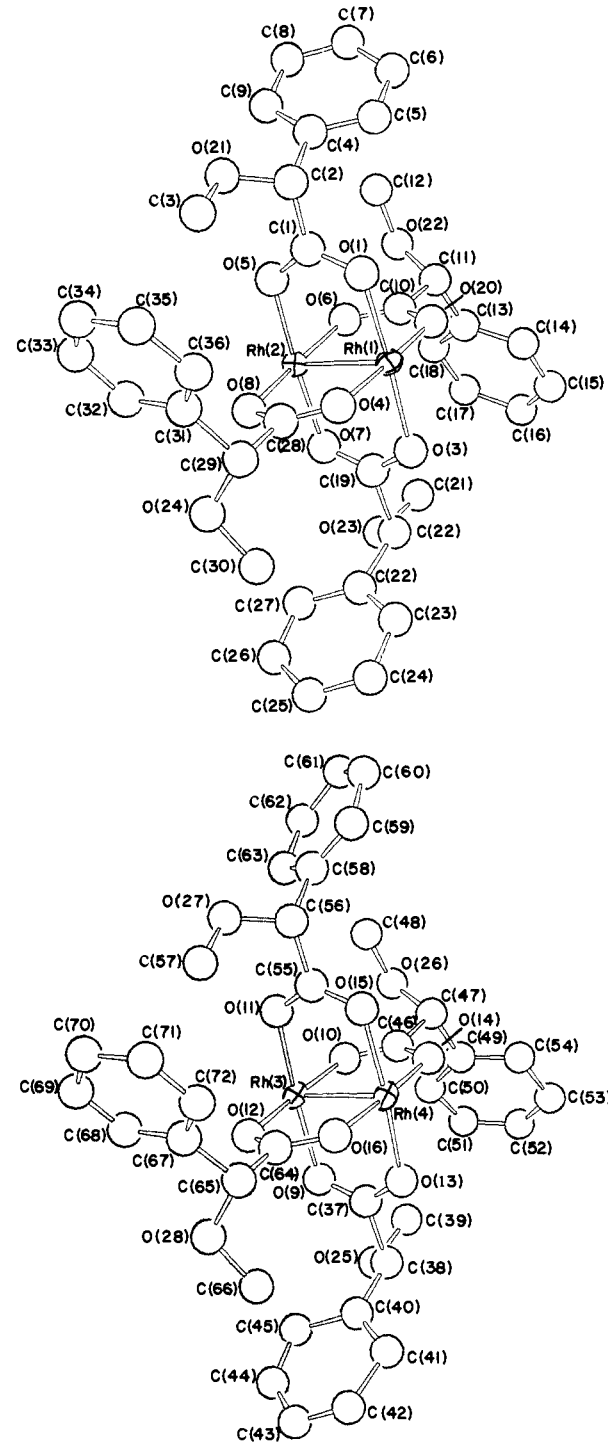

Figure 2. ORTEP drawings of (a) molecule 1 and (b) molecule 2 from the crystal structure of $Rh_2((R)$-α-methoxy-α-phenylacetate$)_4(THF)_2$, **2**, showing the molecular structures and atom labeling schemes. The axial THF ligands have been omitted for clarity.

explicitly stated the connection between the (*d*,*l*)- and (*R*,*S*)-designations for mandelic acid. We have previously established the identities of the (D,L)-designations (not to be confused with the lower case (*d*,*l*)-designations) in a structural study[21] of the quadruply bonded complex $Mo_2[(R)$-mand$]_4$. As a result of our structural studies, we can state that all of the designations *d*, (+), *L*, and *S* belong to one isomer, while *l*, (−), D, and *R* belong to the other.

In the structure of **1**, each mandelate ligand has an internal hydrogen bond between the hydroxyl group on C_α and one of the

(21) Cotton, F. A.; Falvello, L. R.; Murillo, C. A. *Inorg. Chem.* **1983**, *22*, 382.

Table I. Crystal Data for $Rh_2((S)\text{-mand})_4(EtOH)_2 \cdot 0.43EtOH$ (**1**) and $Rh_2((R)\text{-mpa})_4(THF)_2$ (**2**)

	1	**2**
formula	$Rh_2O_{14.4}C_{36.9}H_{42.6}$	$Rh_2O_{14}C_{44}H_{52}$
formula wt	922.3	1010.7
space group	$P2_12_12_1$	$P\bar{1}$
systematic absences	($h00$): $h = 2n + 1$; ($0k0$): $k = 2n + 1$; ($00l$): $l = 2n + 1$	
a, Å	9.027 (2)	11.263 (2)
b, Å	27.110 (5)	20.544 (3)
c, Å	32.656 (5)	10.325 (2)
α, deg	90.0	91.83 (1)
β, deg	90.0	110.21 (1)
γ, deg	90.0	89.11 (1)
V, Å^3	7992 (4)	2234.5 (6)
Z	8	2
d_{calcd}, g/cm^3	1.53	1.50
cryst size, mm	0.5 × 0.2 × 0.1	0.4 × 0.4 × 0.2
μ(Mo Kα), cm^{-1}	8.72	7.87
data collectn instrmt	Enraf–Nonius CAD-4F	Nicolet P3/F
radiatn (monochromated in incident beam)	Mo Kα (λ_α = 0.71073 Å)	
orientatn reflcs, no., range (2θ)	25; 17–29°	25; 21–30°
scan method	$\omega - 2\theta$ scans	ω scans
data col. range, 2θ, deg	4.0–46.0	4.0–50.0
no. of unique data, total	9979	10435
with $F_o^2 > 3\sigma(F_o^2)$	5890	6516
no. of params refind	939	1078
trans, factors, max., min.	obsd 1.00, 0.96; calcd 0.92, 0.62	obsd 1.00, 0.91; calcd 0.85, 0.62
R^a	0.0455	0.0460
$R_w{}^b$	0.0551	0.0543
qual-of-fit indctr^c	1.026	1.004
larg shift/esd, fin. cycle	0.20	0.27
larg peak, e/Å^3	0.95	0.81

$^a R = \sum||F_o| - |F_c||/\sum|F_o|$. $^b R_w = [\sum w(|F_o| - |F_c|)^2/\sum w|F_o|^2]^{1/2}$; $w = 1/\sigma^2(|F_o|)$. ^{c} Quality-of-fit $= [\sum w(|F_o| - |F_c|)^2/(N_{obsd} - N_{params})]^{1/2}$.

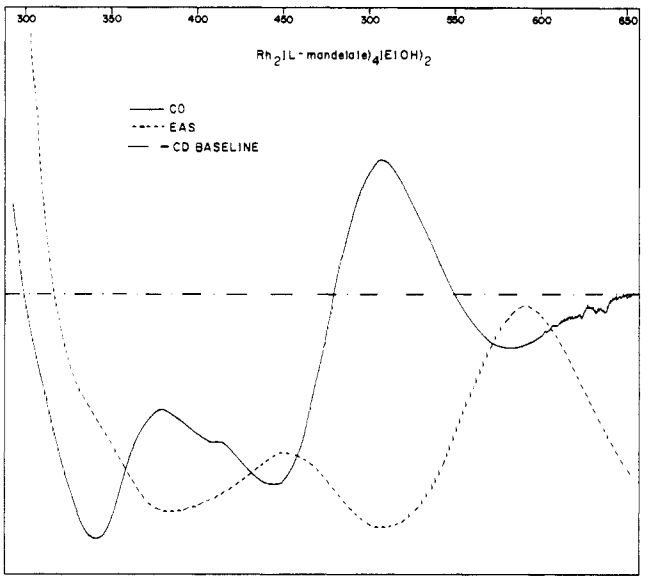

Figure 3. Composite electronic and circular dichroism spectra of $Rh_2((S)\text{-mandelate})_4(EtOH)_2$, **1**, in the range 650–300 nm. Both spectra were taken from the same ethanol solution of the complex at room temperature.

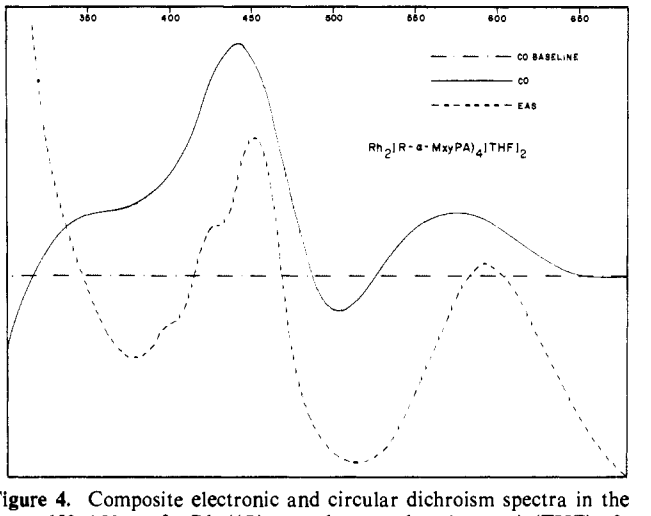

Figure 4. Composite electronic and circular dichroism spectra in the range 650–350 nm for $Rh_2((R)\text{-}\alpha\text{-methoxy-}\alpha\text{-phenylacetate})_4(THF)_2$, **2**. Both spectra were taken at room temperature, from the same THF solution of the complex.

coordinated carboxyl oxygen atoms. The average hydrogen-bond distance is 2.64 [1] Å.[22] The presence of axial ethanol ligands prevents the sort of complex intermolecular interactions which were observed[21] in the structure of $Mo_2[(R)\text{-mand}]_4 \cdot 2THF$. The intraligand hydrogen bonds limit rotation about the C(carboxyl)–C_α bond, in such a way that the C_α–O(H) bond lies near the plane of the carboxyl group. (See Figure 1.)

In the structure of **2**, in which the –OH groups of the mandelate are replaced by methoxy groups, there is no hydrogen bonding. Thus, there is no electronic restriction on rotation about the C(carboxyl)–C_α bond; and the observed paddlewheel arrangement of the four phenyl groups in each molecule is the result of intramolecular steric repulsions and crystal-packing forces.

Spectroscopic Results. The solution electronic and circular dichroism (CD) spectra of compounds **1** and **2** are shown in Figures 3 and 4, respectively. The visible spectra of both complexes show the two predominant peaks characteristic of the dirhodium tetracarboxylates.

Compound **1** has maxima in the visible region at 585 (17 100 cm^{-1}, ϵ = 190) and at 445 nm (22 500 cm^{-1}, ϵ = 110) in the electronic spectrum. In the circular dichroism spectrum there are negative peaks corresponding to the observed electronic transitions. In addition, there is a positive CD transition at ~500 nm. This peak does not correspond directly to any of the transitions in the electronic spectrum.

The visible region of the electronic spectrum of **2** has peaks at 593 (16 900 cm^{-1}, ϵ = 212) and 450 nm (22 200 cm^{-1}, ϵ = 314) as well as two shoulders at 425 nm (23 500 cm^{-1}) and 400 nm

(22) The deviation reported in square brackets is calculated as

$$[\sum_n \Delta_i^2/n(n-1)]^{1/2}$$

in which Δ_i is the deviation of the ith (of n) values from the mean of the set.

Table II. Atomic Positional Parameters and Equivalent Isotropic Displacement Parameters (Å^2) and Their Estimated Standard Deviations for Rh_2((*S*)-mandelate)$_4$(EtOH)$_2$·0·43EtOH (**1**)[b]

atom	x	y	z	B (Å^2)	atom	x	y	z	B (Å^2)
Rh(1)	0.1499 (1)	0.39424 (3)	0.17872 (3)	2.49 (2)	C(23)	−0.274 (2)	0.2269 (5)	0.1690 (6)	7.1 (5)
Rh(2)	−0.0002 (1)	0.45523 (3)	0.14627 (3)	2.58 (2)	C(24)	−0.258 (2)	0.2684 (5)	0.1991 (6)	6.8 (5)
Rh(3)	−0.1494 (1)	0.48156 (4)	0.34774 (3)	3.03 (2)	C(25)	0.133 (1)	0.4854 (4)	0.2225 (3)	2.8 (3)
Rh(4)	−0.3038 (1)	0.41410 (4)	0.32824 (3)	2.81 (2)	C(26)	0.163 (1)	0.5210 (4)	0.2569 (3)	3.2 (3)
O(1)	0.3268 (8)	0.4220 (3)	0.1490 (2)	3.5 (2)	C(27)	0.156 (1)	0.5741 (5)	0.2435 (4)	3.8 (3)
O(2)	0.1032 (9)	0.3492 (3)	0.1316 (2)	3.7 (2)	C(28)	0.050 (2)	0.6046 (5)	0.2591 (5)	6.4 (5)
O(3)	−0.0369 (8)	0.3688 (3)	0.2064 (3)	3.2 (2)	C(29)	0.041 (2)	0.6535 (6)	0.2456 (6)	8.4 (6)
O(4)	0.1870 (9)	0.4426 (3)	0.2247 (2)	2.9 (2)	C(30)	0.137 (2)	0.6714 (5)	0.2173 (6)	7.6 (5)
O(5)	0.1862 (8)	0.4801 (3)	0.1175 (2)	3.1 (2)	C(31)	0.250 (2)	0.6416 (6)	0.1986 (6)	6.9 (5)
O(6)	−0.039 (1)	0.4058 (3)	0.1000 (3)	4.3 (2)	C(32)	0.256 (2)	0.5919 (5)	0.2136 (5)	5.1 (4)
O(7)	−0.1799 (8)	0.4262 (3)	0.1746 (2)	3.2 (2)	C(33)	0.003 (1)	0.4010 (4)	0.3111 (3)	3.0 (3)
O(8)	0.0454 (9)	0.4997 (3)	0.1944 (2)	2.9 (2)	C(34)	0.135 (1)	0.3674 (4)	0.3022 (4)	3.2 (3)
O(9)	0.5677 (9)	0.4765 (3)	0.1334 (3)	4.5 (2)	C(35)	0.148 (1)	0.3329 (5)	0.3398 (4)	4.4 (3)
O(10)	−0.116 (1)	0.3449 (4)	0.0415 (3)	9.6 (4)	C(36)	0.096 (2)	0.2836 (5)	0.3328 (6)	7.9 (5)
O(11)	−0.427 (1)	0.3870 (3)	0.2077 (2)	3.6 (2)[a]	C(37)	0.106 (2)	0.2533 (6)	0.3693 (7)	11.2 (6)
O(12)	0.3026 (9)	0.5093 (3)	0.2740 (2)	3.4 (2)	C(38)	0.172 (2)	0.2701 (8)	0.4037 (6)	10.6 (7)
O(13)	0.0262 (8)	0.4432 (3)	0.3260 (2)	2.9 (2)	C(39)	0.230 (2)	0.317 (1)	0.4093 (6)	10.9 (7)
O(14)	−0.1896 (8)	0.5119 (3)	0.2918 (2)	3.3 (2)	C(40)	0.216 (2)	0.3510 (6)	0.3740 (4)	6.3 (4)
O(15)	−0.338 (1)	0.5160 (3)	0.3696 (2)	4.6 (2)	C(41)	−0.282 (1)	0.4905 (4)	0.2694 (3)	2.7 (3)
O(16)	−0.118 (1)	0.4486 (3)	0.4029 (3)	4.9 (2)	C(42)	−0.325 (1)	0.5192 (4)	0.2303 (3)	3.0 (3)
O(17)	−0.1207 (9)	0.3804 (3)	0.3055 (2)	3.4 (2)	C(43)	−0.346 (2)	0.5735 (5)	0.2359 (4)	4.6 (3)
O(18)	−0.3435 (9)	0.4502 (3)	0.2745 (2)	3.2 (2)	C(44)	−0.313 (2)	0.6024 (6)	0.2018 (6)	8.2 (5)
O(19)	−0.4782 (9)	0.4509 (3)	0.3527 (3)	4.0 (2)	C(45)	−0.345 (3)	0.6547 (7)	0.2064 (7)	11.4 (7)
O(20)	−0.257 (1)	0.3833 (3)	0.3832 (3)	4.6 (2)	C(46)	−0.394 (2)	0.6755 (6)	0.2421 (7)	10.5 (6)
O(21)	0.2710 (9)	0.3961 (3)	0.2995 (3)	3.7 (2)	C(47)	−0.425 (2)	0.6453 (6)	0.2732 (6)	8.8 (6)
O(22)	−0.464 (1)	0.4990 (3)	0.2156 (2)	3.6 (2)	C(48)	−0.403 (2)	0.5935 (5)	0.2711 (5)	5.9 (4)
O(23)	−0.724 (1)	0.5034 (4)	0.3621 (3)	6.8 (3)	C(49)	−0.459 (1)	0.4937 (5)	0.3663 (4)	3.6 (3)
O(24)	−0.064 (1)	0.4130 (5)	0.4739 (3)	9.0 (3)	C(50)	−0.595 (1)	0.5218 (5)	0.3794 (4)	4.9 (4)
O(25)	0.3010 (9)	0.3389 (3)	0.2107 (3)	3.8 (2)	C(51)	−0.611 (1)	0.5199 (5)	0.4260 (4)	4.5 (3)
O(26)	−0.149 (1)	0.5155 (3)	0.1182 (3)	5.6 (2)	C(52)	−0.535 (3)	0.5551 (9)	0.4484 (7)	15.1 (7)
O(27)	0.009 (1)	0.5443 (3)	0.3633 (3)	5.6 (2)	C(53)	−0.549 (3)	0.550 (1)	0.4949 (6)	20.7 (9)
O(28)	−0.4584 (9)	0.3521 (3)	0.3075 (2)	3.6 (2)	C(54)	−0.650 (2)	0.514 (1)	0.4995 (8)	18.9 (9)
C(1)	0.308 (1)	0.4583 (5)	0.1256 (4)	3.3 (3)	C(55)	−0.707 (4)	0.483 (1)	0.493 (1)	27 (1)
C(2)	0.448 (1)	0.4812 (5)	0.1048 (3)	3.6 (3)	C(56)	−0.696 (2)	0.4874 (9)	0.4427 (5)	10.0 (6)
C(3)	0.496 (2)	0.4512 (5)	0.0668 (3)	4.3 (3)	C(57)	−0.170 (2)	0.4068 (5)	0.4082 (3)	4.1 (3)
C(4)	0.453 (2)	0.4021 (6)	0.0618 (4)	6.4 (5)	C(58)	−0.128 (2)	0.3784 (6)	0.4467 (4)	6.2 (5)
C(5)	0.510 (2)	0.3767 (6)	0.0260 (5)	7.4 (5)	C(59)	−0.270 (2)	0.3570 (5)	0.4664 (4)	5.6 (4)
C(6)	0.599 (2)	0.4037 (9)	−0.0029 (6)	10.9 (7)	C(60)	−0.379 (2)	0.3877 (7)	0.4843 (5)	8.4 (5)
C(7)	0.627 (2)	0.4545 (8)	0.0031 (5)	9.2 (6)	C(61)	−0.505 (3)	0.3666 (8)	0.5024 (7)	11.5 (7)
C(8)	0.573 (2)	0.4783 (7)	0.0384 (5)	7.1 (5)	C(62)	−0.518 (3)	0.3169 (8)	0.5058 (6)	10.7 (7)
C(9)	0.018 (1)	0.3644 (5)	0.1047 (4)	4.3 (3)	C(63)	−0.417 (3)	0.2846 (8)	0.4871 (7)	13.1 (9)
C(10)	−0.039 (2)	0.3242 (6)	0.0750 (5)	6.9 (4)	C(64)	−0.281 (2)	0.3066 (7)	0.4670 (5)	9.2 (6)
C(11)	0.087 (2)	0.2900 (6)	0.0607 (5)	7.6 (5)	C(65)	0.307 (2)	0.2870 (4)	0.1937 (5)	5.8 (4)
C(12)	0.159 (2)	0.3005 (8)	0.0251 (5)	12.2 (6)	C(66)	0.162 (2)	0.2636 (5)	0.2035 (5)	6.7 (5)
C(13)	0.284 (3)	0.270 (1)	0.0073 (8)	17 (1)	C(67)	−0.113 (2)	0.5557 (7)	0.0923 (5)	8.5 (5)
C(14)	0.299 (2)	0.2306 (7)	0.0335 (5)	17.7 (5)	C(68)	−0.010 (3)	0.5890 (7)	0.1125 (7)	10.1 (6)
C(15)	0.237 (3)	0.2162 (8)	0.0722 (8)	13.1 (8)	C(69)	−0.026 (2)	0.5823 (6)	0.3886 (8)	13.2 (6)
C(16)	0.115 (2)	0.2497 (6)	0.0859 (6)	9.2 (6)	C(70)	0.081 (3)	0.6192 (8)	0.3915 (9)	14.1 (9)
C(17)	−0.161 (1)	0.3897 (4)	0.1959 (3)	2.8 (3)	C(71)	−0.461 (2)	0.3038 (6)	0.3264 (8)	11.1 (7)
C(18)	−0.296 (1)	0.3587 (4)	0.2119 (3)	2.7 (2)[a]	C(72)	−0.336 (2)	0.2782 (7)	0.3325 (8)	11.6 (7)
C(19)	−0.313 (1)	0.3140 (4)	0.1836 (4)	3.5 (3)	O(29)	0.495	0.601	0.060	24.5
C(20)	−0.376 (2)	0.3193 (5)	0.1453 (4)	4.7 (4)	C(73)	0.408	0.647	0.063	23.8
C(21)	−0.388 (2)	0.2782 (6)	0.1177 (5)	7.0 (5)	C(74)	0.524	0.659	0.081	20.2
C(22)	−0.340 (2)	0.2317 (6)	0.1340 (5)	7.4 (5)					

[a] Atoms were refined isotropically. [b] Anisotropically refined atoms are given in the form of the equivalent isotropic displacement parameter defined as $^4/_3[a^2\beta_{11} + b^2\beta_{22} + c^2\beta_{33} + ab(\cos\gamma)\beta_{12} + ac(\cos\beta)\beta_{13} + bc(\cos\alpha)\beta_{23}]$. Atoms of the lattice ethanol were not included in the last cycle, and so no esd's of their parameters are reported.

(25 000 cm^{-1}). The shoulder at 400 nm has also been observed in the spectrum of $Rh_2(O_2CCH_3)_4(H_2O)_2$.[13] The CD spectrum of **2** has positive bands at 575 and 440 nm, corresponding to the bands in the electronic spectrum, and a negative peak at 500 nm. Thus, the CD spectra of **1** and **2** are qualitatively similar. The major difference is that the corresponding peaks in the two spectra are opposite in sign; this was expected, since the two compounds have ligands with opposite absolute configurations.

Interpretation of the CD Spectra. Our discussion of the CD spectra of compounds **1** and **2** will focus on three major points: (a) the origin of the CD peaks in the regions near 600 and 450 nm, i.e., those peaks corresponding in energy to the prominent peaks in the electronic spectrum; (b) the relative signs of these two CD bands; and (c) the origin and sign of the CD band at 500 nm in each spectrum. Our analysis of the CD spectra develops logically in relationship to the more recent assignment[13] of the electronic spectrum of the dirhodium tetracarboxylates. We have not uncovered a sensible interpretation of the CD spectra which can be related to the earlier assignments[5,6] of the electronic transitions.

(a) Origin of the CD Peaks Near 600 and 450 nm. Compounds **1** and **2** fall into the category of the "case II" chromophore[23]—that is, an intrinsically achiral chromophore which gives rise to chiroptical effects through perturbation by chiral surroundings. The transitions under consideration do not involve electronic promotions within the chiral environment or between the chromophore and the chiral environment.

Circular dichroism arises when the promotion of an electron involves both electric and magnetic moments, such that the two moments are not orthogonal.[24] The "rotational strength" of a

(23) Moscowitz, A. *Tetrahedron* **1961**, *13*, 48.

Table III. Atomic Positional Parameters and Equivalent Isotropic Displacement Parameters (Å^2) and Their Estimated Standard Deviations for Rh_2((*R*)-α-methoxy-α-phenylacetate)$_4$(THF)$_2$ (**2**)[a]

atom	*x*	*y*	*z*	*B* (Å^2)	atom	*x*	*y*	*z*	*B* (Å^2)
Rh(1)	0.000	0.000	0.000	2.28 (2)	C(29)	−0.409 (1)	−0.0096 (7)	−0.128 (1)	4.1 (3)
Rh(2)	−0.04895 (9)	0.02605 (5)	0.20325 (9)	2.25 (2)	C(30)	−0.453 (2)	0.0995 (8)	−0.179 (2)	7.4 (5)
Rh(3)	0.98799 (9)	0.52988 (5)	0.5741 (1)	2.53 (2)	C(31)	−0.456 (1)	−0.0701 (6)	−0.072 (1)	3.7 (3)
Rh(4)	0.95324 (9)	0.50008 (5)	0.7799 (1)	2.72 (2)	C(32)	−0.483 (1)	−0.0651 (7)	0.051 (1)	4.9 (3)
O(1)	0.0150 (7)	−0.0946 (4)	0.0548 (8)	3.3 (2)	C(33)	−0.528 (2)	−0.1211 (8)	0.093 (2)	6.0 (4)
O(2)	0.1837 (7)	0.0126 (4)	0.1129 (8)	3.2 (2)	C(34)	−0.552 (1)	−0.1793 (7)	0.016 (2)	5.1 (4)
O(3)	−0.0172 (8)	0.0983 (4)	−0.0431 (8)	3.4 (2)	C(35)	−0.523 (1)	−0.1853 (7)	−0.102 (2)	5.3 (4)
O(4)	−0.1886 (7)	−0.0124 (4)	−0.1037 (7)	3.0 (2)	C(36)	−0.474 (1)	−0.1311 (6)	−0.153 (1)	4.2 (3)
O(5)	−0.0378 (7)	−0.0708 (4)	0.2405 (7)	2.8 (2)	C(37)	0.808 (1)	0.4290 (5)	0.537 (1)	3.6 (3)
O(6)	0.1427 (7)	0.0331 (4)	0.3070 (8)	3.5 (2)	C(38)	0.713 (1)	0.3728 (7)	0.462 (1)	5.1 (3)
O(7)	−0.0552 (7)	0.1215 (3)	0.1548 (8)	2.9 (2)	C(39)	0.873 (2)	0.3037 (9)	0.426 (2)	7.7 (5)
O(8)	−0.2363 (7)	0.0166 (4)	0.0864 (8)	3.4 (2)	C(40)	0.586 (1)	0.4002 (7)	0.392 (2)	6.2 (4)
O(9)	0.8554 (8)	0.4611 (4)	0.4695 (8)	3.6 (2)	C(41)	0.490 (2)	0.3967 (9)	0.452 (2)	7.9 (5)
O(10)	1.1270 (8)	0.4604 (4)	0.6162 (8)	3.8 (2)	C(42)	0.361 (2)	0.426 (1)	0.363 (3)	13.8 (8)
O(11)	1.1143 (7)	0.5965 (4)	0.6913 (8)	3.1 (2)	C(43)	0.337 (2)	0.444 (1)	0.236 (2)	11.6 (7)
O(12)	0.8442 (7)	0.5973 (4)	0.5445 (8)	3.1 (2)	C(44)	0.431 (2)	0.447 (1)	0.192 (2)	10.5 (7)
O(13)	0.8243 (8)	0.4357 (4)	0.6631 (8)	3.9 (2)	C(45)	0.554 (2)	0.430 (1)	0.259 (2)	7.5 (5)
O(14)	1.0932 (8)	0.4330 (4)	0.8102 (8)	4.0 (2)	C(46)	1.154 (1)	0.4299 (6)	0.725 (1)	3.8 (3)
O(15)	1.0833 (8)	0.5689 (4)	0.8852 (7)	3.4 (2)	C(47)	1.266 (1)	0.3827 (7)	0.768 (2)	4.9 (4)
O(16)	0.8146 (7)	0.5699 (4)	0.7403 (9)	3.7 (2)	C(48)	1.421(2)	0.4596 (9)	0.759 (2)	8.1 (6)
O(17)	0.0532 (8)	−0.0220 (4)	−0.1902 (8)	3.6 (2)	C(49)	1.223 (1)	0.3127 (7)	0.708 (2)	5.8 (4)
O(18)	−0.1094 (8)	0.0506 (4)	0.3919 (8)	4.0 (2)	C(50)	1.191 (2)	0.2960 (9)	0.571 (2)	6.9 (5)
O(19)	1.0269 (8)	0.5614 (4)	0.3824 (8)	3.8 (2)	C(51)	1.162 (2)	0.227 (1)	0.537 (2)	8.5 (6)
O(20)	0.9163 (9)	0.4702 (5)	0.9738 (9)	5.2 (2)	C(52)	1.161 (2)	0.1846 (9)	0.634 (2)	11.2 (6)
O(21)	−0.0912 (8)	−0.2025 (4)	0.2459 (8)	3.7 (2)	C(53)	1.179 (2)	0.2054 (9)	0.772 (2)	11.6 (6)
O(22)	0.3947 (9)	0.0179 (5)	0.4606 (9)	4.8 (2)	C(54)	1.223 (2)	0.2736 (9)	0.817 (2)	8.6 (5)
O(23)	0.0105 (9)	0.2493 (4)	0.128 (1)	4.8 (3)	C(55)	1.133 (1)	0.6040 (6)	0.821 (1)	3.1 (3)
O(24)	−0.4792 (8)	0.0424 (5)	−0.109 (1)	4.8 (2)	C(56)	1.219 (1)	0.6600 (6)	0.902 (1)	3.7 (3)
O(25)	0.7548 (9)	0.3388 (4)	0.3626 (9)	4.7 (2)	C(57)	1.080 (2)	0.7410 (8)	0.778 (2)	7.5 (6)
O(26)	1.3560 (9)	0.3999 (5)	0.702 (1)	5.7 (3)	C(58)	1.359 (1)	0.6396 (6)	0.951 (1)	4.0 (3)
O(27)	1.2045 (9)	0.7148 (4)	0.818 (1)	5.0 (3)	C(59)	1.424 (1)	0.6398 (8)	1.087 (2)	5.5 (4)
O(28)	0.5932 (9)	0.6416 (4)	0.470 (1)	5.0 (3)	C(60)	1.555 (2)	0.628 (1)	1.132 (2)	7.6 (6)
C(1)	−0.007 (1)	−0.1119 (5)	0.163 (1)	3.0 (3)	C(61)	1.618 (2)	0.6106 (9)	1.037 (2)	6.9 (5)
C(2)	−0.000 (1)	0.1844 (5)	0.187 (1)	3.0 (3)	C(62)	1.542 (1)	0.6089 (8)	0.898 (2)	5.7 (4)
C(3)	−0.220 (1)	−0.2027 (8)	0.142 (2)	5.6 (4)	C(63)	1.412 (1)	0.6267 (7)	0.851 (1)	4.2 (3)
C(4)	0.130 (1)	−0.2011 (5)	0.293 (1)	2.9 (3)	C(64)	0.789 (1)	0.6035 (6)	0.630 (1)	2.8 (2)
C(5)	0.230 (1)	−0.2033 (7)	0.245 (1)	4.1 (3)	C(65)	0.684 (1)	0.6529 (6)	0.608 (1)	3.7 (3)
C(6)	0.353 (1)	−0.2200 (8)	0.340 (2)	6.5 (5)	C(66)	0.524 (2)	0.5808 (9)	0.463 (2)	7.9 (6)
C(7)	0.369 (2)	−0.2324 (7)	0.477 (2)	5.3 (4)	C(67)	0.725 (1)	0.7228 (6)	0.614 (1)	2.8 (2)
C(8)	0.266 (1)	−0.2285 (8)	0.517 (2)	5.1 (4)	C(68)	0.753 (1)	0.7508 (7)	0.503 (1)	5.1 (3)
C(9)	0.143 (1)	−0.2108 (6)	0.428 (1)	4.4 (4)	C(69)	0.789 (2)	0.8154 (8)	0.518 (2)	7.0 (5)
C(10)	0.215 (1)	0.0246 (5)	0.241 (1)	2.6 (2)	C(70)	0.809 (2)	0.8520 (7)	0.642 (2)	5.9 (4)
C(11)	0.356 (1)	0.0324 (6)	0.313 (1)	3.3 (3)	C(71)	0.787 (2)	0.8232 (7)	0.753 (2)	5.7 (4)
C(12)	0.384 (1)	−0.0499 (7)	0.485 (2)	4.9 (4)	C(72)	0.748 (1)	0.7570 (7)	0.739 (1)	5.2 (4)
C(13)	0.395 (1)	0.0992 (7)	0.300 (1)	4.0 (3)	C(73)	0.132 (1)	−0.0797 (6)	−0.182 (1)	4.2 (3)
C(14)	0.436 (2)	0.1144 (8)	0.188 (2)	6.1 (5)	C(74)	0.175 (2)	−0.0766 (7)	−0.308 (2)	5.7 (4)
C(15)	0.470 (2)	0.1766 (8)	0.168 (2)	7.7 (6)	C(75)	0.182 (1)	−0.0006 (7)	−0.322 (2)	5.2 (4)
C(16)	0.473 (2)	0.2277 (9)	0.265 (2)	7.5 (6)	C(76)	0.111 (1)	0.0308 (7)	−0.235 (1)	4.7 (3)
C(17)	0.438 (2)	0.2119 (8)	0.382 (2)	6.3 (5)	C(77)	−0.177 (2)	0.1131 (7)	0.387 (2)	6.9 (5)
C(18)	0.400 (2)	0.1483 (7)	0.407 (2)	6.3 (5)	C(78)	−0.229 (2)	0.108 (1)	0.498 (2)	7.8 (5)
C(19)	−0.038 (1)	0.1360 (5)	0.047 (1)	2.9 (3)	C(79)	−0.252 (1)	0.036 (1)	0.512 (2)	7.9 (5)
C(20)	−0.043 (1)	0.2083 (6)	0.006 (1)	3.5 (3)	C(80)	−0.181 (1)	−0.0001 (7)	0.430 (2)	5.9 (4)
C(21)	0.148 (2)	0.246 (1)	0.183 (2)	8.9 (6)	C(81)	0.950 (2)	0.614 (1)	0.302 (2)	7.2 (5)
C(22)	−0.183 (1)	0.2299 (7)	−0.061 (1)	4.3 (3)	C(82)	1.003 (2)	0.6290 (8)	0.196 (1)	6.0 (4)
C(23)	−0.258 (2)	0.2474 (8)	0.019 (2)	7.0 (4)	C(83)	1.145 (1)	0.6113 (9)	0.263 (2)	6.2 (4)
C(24)	−0.378 (2)	0.271 (1)	−0.052 (3)	10.7 (8)	C(84)	1.157 (2)	0.575 (1)	0.394 (2)	8.9 (6)
C(25)	−0.421 (2)	0.2704 (8)	−0.206 (2)	9.0 (5)	C(85)	0.990 (2)	0.425 (1)	1.065 (2)	11.7 (7)
C(26)	−0.345 (2)	0.252 (1)	−0.280 (2)	11.0 (7)	C(86)	0.930 (2)	0.411 (1)	1.165 (2)	8.3 (6)
C(27)	−0.222 (2)	0.2278 (9)	−0.205 (2)	7.1 (5)	C(87)	0.803 (2)	0.434 (1)	1.107 (2)	10.2 (6)
C(28)	−0.262 (1)	−0.0009 (5)	−0.042 (1)	3.0 (3)	C(88)	0.788 (1)	0.454 (1)	0.953 (2)	8.7 (6)

[a] Anisotropically refined atoms are given in the form of the equivalent isotropic displacement parameter defined as $^4/_3[a^2\beta_{11} + b^2\beta_{22} + c^2\beta_{33} + ab(\cos\gamma)\beta_{12} + ac(\cos\beta)\beta_{13} + bc(\cos\alpha)\beta_{23}]$.

transition is the scalar product of the magnetic and electric moments of the transition, as in eq 1, in which Im signifies the

$$R = \mathrm{Im} \langle a|P|b \rangle \langle b|M|a \rangle = \mu m \cos\theta \qquad (1)$$

imaginary part of the product; *P* and *M* are the electric and magnetic dipole operators,respectively; *a* and *b* represent the orbitals involved in the transition; μ and *m* are the electric dipole and magnetic moments associated with the transition; and θ is the angle between the two moments. If θ is acute, the CD transition has a positive sign, whereas an obtuse θ gives a negative CD.

In order for a CD transition to occur, both of the matrix elements in eq 1 must be nonzero. Group theory can be applied to identify the nonvanishing integrals.[25] In the case of a chiral

(24) Mason, S. F. *Q. Rev., Chem. Soc.* **1963**, *17*, 20.

(25) Cotton, F. A. "Chemical Applications of Group Theory", 2nd ed.; Wiley-Interscience: New York, **1963**; pp 101–104.

Table IV. Selected Bond Distances (Å) and Angles (deg) and Their Estimated Standard Deviations[a] for $Rh_2((S)$-mandelate$)_4(EtOH)_2 \cdot 0.43EtOH$ (**1**)

atom	distance (Å)	atom	distance (Å)
Rh(1)-Rh(2)	2.386 (2)	Rh(3)-O(16)	2.029 (10)
-O(1)	2.016 (9)	-O(27)	2.281 (11)
-O (2)	2.010 (9)	Rh(4)-O(17)	2.030 (10)
-O(3)	2.034 (9)	-O(18)	2.040 (9)
-O(4)	2.021 (8)	-O(19)	2.027 (10)
-O(25)	2.279 (9)	-O(20)	2.023 (10)
Rh(2)-O(5)	2.041 (8)	-O(28)	2.287 (9)
-O(6)	2.048 (9)	O(1)-O(9)	2.677 (13)
-O(7)	2.027 (9)	O(4)-O(12)	2.636 (12)
-O(8)	2.024 (8)	O(6)-O(10)	2.622 (15)
-O(26)	2.303 (10)	O(7)-O(11)	2.694 (13)
Rh(3)-Rh(4)	2.386 (2)	O(13)-O(21)	2.693 (13)
-O(13)	2.026 (9)	O(16)-O(24)	2.56 (2)
-O(14)	2.035 (9)	O(18)-O(22)	2.574 (12)
-O(15)	2.067 (10)	O(19)-O(23)	2.658 (15)

atom	angle (deg)	atom	angle (deg)
Rh(2)-Rh(1)-O(1)	88.7 (3)	Rh(4)-Rh(3)-O(13)	88.2 (2)
-O(2)	87.8 (3)	-O(14)	88.1 (3)
-O(3)	87.8 (3)	-O(15)	87.6 (3)
-O(4)	88.5 (3)	-O(16)	88.9 (3)
-O(25)	177.2 (2)	-O(27)	176.2 (3)
Rh(1)-Rh(2)-O(5)	88.0 (3)	Rh(3)-Rh(4)-O(17)	88.2 (3)
-O(6)	88.4 (3)	-O(18)	88.0 (3)
-O(7)	89.0 (3)	-O(19)	88.4 (3)
-O(8)	87.3 (3)	-O(20)	87.6 (3)
-O(26)	177.1 (3)	-O(28)	177.1 (3)

[a] Estimated standard deviations in the least significant digits are given in parentheses.

Table V. Selected Bond Distances (Å) and Angles (deg) and Their Estimated Standard Deviations[a] for $Rh_2((R)$-α-methoxy-α-phenylacetate$)_4(THF)_2$ (**2**)

atom	distance (Å)	atom	distance (Å)
Rh(1)-Rh(2)	2.391 (1)	Rh(3)-Rh(4)	2.389 (1)
-O(1)	2.030 (10)	-O(9)	2.061 (10)
-O(2)	2.009 (10)	-O(10)	2.044 (10)
-O(3)	2.074 (10)	-O(11)	2.032 (10)
-O(4)	2.037 (9)	-O(12)	2.062 (10)
-O(17)	2.274 (11)	-O(19)	2.284 (11)
Rh(2)-O(5)	2.031 (10)	Rh(4)-O(13)	2.016 (10)
-O(6)	2.056 (11)	-O(14)	2.025 (10)
-O(7)	2.033 (9)	-O(15)	2.048 (9)
-O(8)	2.045 (10)	-O(16)	2.046 (10)
-O(18)	2.315 (10)	-O(20)	2.284 (12)

atom	angle (deg)	atom	angle (deg)
Rh(2)-Rh(1)-O(1)	87.9 (3)	Rh(4)-Rh(3)-O(9)	87.7 (3)
-O(2)	88.3 (3)	-O(10)	87.8 (3)
-O(3)	88.1 (3)	-O(11)	87.6 (3)
-O(4)	88.3 (3)	-O(12)	87.7 (3)
-O(17)	177.7 (3)	-O(19)	177.7 (3)
Rh(1)-Rh(2)-O(5)	87.6 (3)	Rh(3)-Rh(4)-O(13)	87.7 (3)
-O(6)	87.2 (3)	-O(14)	88.4 (3)
-O(7)	88.3 (3)	-O(15)	88.2 (3)
-O(8)	88.2 (3)	-O(16)	88.4 (3)
-O(18)	176.5 (3)	-O(20)	178.7 (3)

[a] Estimated standard deviations in the least significant digits are given in parentheses.

chromophore any allowed electronic transition has both electric and magnetic moments, and so any transition observed in the electronic spectrum will also be seen in the CD spectrum. In the case of the dirhodium tetracarboxylates, however, the $Rh_2(O_{eq})_8(O_{ax})_2$ chromophore has D_{4h} symmetry (or D_{2h} symmetry if the anisotropy of the axial ligands is taken into account). In these point groups (and in all other common achiral point groups except S_4 and the C_{nv} groups), no transition can be strictly allowed both electronically and magnetically.

In order to explain the circular dichroism from compounds **1** and **2**, we invoke the one-electron, static-coupling mechanism, which has been discussed by Mason[26] and by Schellman.[27,28] With

Table VI. Average Bond Distances (Å) and Angles (deg) and Their Estimated Standard Deviations[a] for $Rh_2((S)$-mandelate$)_4(EtOH)_2 \cdot 0.43EtOH$ (**1**) and $Rh_2((R)$-α-methoxy-α-phenylacetate$)_4(THF)_2$ (**2**)

	1	**2**
	Distances	
Rh-Rh	2.386 [2]	2.390 [1]
Rh-O_{eq}	2.031 [3]	2.041 [4]
Rh-O_{ax}	2.295 [7]	2.289 [9]
O_{eq}-C	1.26 [1]	1.26 [1]
C-C_α	1.54 [1]	1.54 [1]
C_α-O	1.42 [1]	1.43 [1]
C_α-C_β	1.53 [1]	1.53 [1]
O-C_{Me}		1.45 [1]
O(H)···O_{eq}	2.64 [1]	
	Angles	
Rh-Rh-O_{eq}	88.2 [2]	88.0 [1]
Rh-Rh-O_{ax}	176.9 [2]	177.7 [5]
Rh-O_{eq}-C	118.1 [3]	119 [1]
O_{eq}-C-O_{eq}	127 [1]	126 [1]
O_{eq}-C-C_α	116 [1]	117 [1]
C-C_α-C_β	110 [1]	110 [1]
C-C_α-O	109 [1]	110 [1]
C_β-C_α-O	108 [1]	107 [1]
C_α-O-C_{Me}		112 [1]

[a] See ref 22 for the definition of the deviation in square brackets.

the assumption stated earlier—that the transitions under consideration do not involve electron transfer between the achiral chromophore and its chiral surroundings—the one-electron mechanism comprises a first-order perturbation mixing of a magnetically accessible excited state into an electronically accessible excited state and vice versa.[29] The perturbation mixing is described by eq 2a and 2b, in which the primed wave functions

$$|M_eL_o\rangle' = |M_eL_o\rangle + \langle M_mL_o|V|M_eL_o\rangle|M_mL_o\rangle(E_e - E_m)^{-1} \quad (2a)$$

$$|M_mL_o\rangle' = |M_mL_o\rangle + \langle M_eL_o|V|M_mL_o\rangle|M_eL_o\rangle(E_m - E_e)^{-1} \quad (2b)$$

represent the perturbed states. The wave functions are represented as $|M_eL_o\rangle$ for the state in which the chromophore (M) is in an electronically accessible excited state, and the surroundings (L) are in the ground state, and as $|M_mL_o\rangle$ for the case in which the chromophore is in a magnetically accessible excited state. The quantities E_m and E_e are the energies of the unperturbed excited states, and the perturbation operator V is an expansion of the potential operator $\sum_L e_M e_L / r_{ML}$. Thus, the mixing of excited states and the appearance of CD effects are caused by the chiral potential surrounding the symmetric chromophore. Equation 2a describes the mixing of a magnetic excited state into an electronically accessible one, and eq 2b describes the reverse process.

A transition from the ground state to one of the perturbed excited states will have both electric and magnetic dipole components and so will give rise to a band in the CD spectrum. A transition which is electric dipole-allowed with dipole moment μ_{oe} acquires, via the perturbation mixing, a magnetic moment m_{eo} described by eq 3a, in which m_{mo} is the magnetic moment of the

$$m_{eo} = m_{mo}\langle M_mL_o|V|M_eL_o\rangle(E_e - E_m)^{-1} \quad (3a)$$

$$\mu_{om} = \mu_{oe}\langle M_eL_o|V|M_mL_o\rangle(E_m - E_e)^{-1} \quad (3b)$$

magnetically allowed transition which is being mixed into the predominantly electronic transition. Similarly, a magnetically allowed transition acquires a small dipole moment μ_{om} by the reverse mixing (eq 3b).

(26) Mason, S. F. In "Optical Activity and Chiral Discrimination"; Mason, S. F., Ed.; D. Reidel: Boston, **1979**; pp 1-24.
(27) Schellman, J. A. *J. Chem. Phys.* **1966**, *44*, 55.
(28) Schellman, J. A. *Acc. Chem. Res.* **1968**, *1*, 144.
(29) An "electronically accessible" excited state is one which results from a transition which is dipole-allowed; i.e., the operator transforms as x, y, or z. A "magnetically accessible" excited state is reached via an allowed transition for which the operator transforms as R_x, R_y, or R_z.

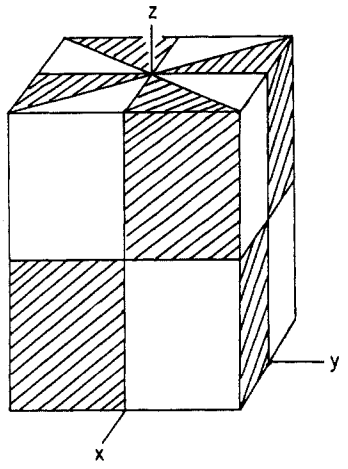

Figure 5. Parity properties of the hexadecapole function ($xyz(x^2 - y^2)$), the lowest order multipole function which transforms as A_{1u} in point group D_{4h}. Sectors in which the function is positive are shaded.

With the acquisition of a magnetic moment, a predominantly electronic transition will have rotational strength R_{oe}, as given by eq 4a. In an analogous fashion, a transition which is magnetically allowed acquires rotational strength R_{om}, given by eq 4b.

$$R_{oe} = \mu_{oe}m_{eo} = \mu_{oe}m_{mo}\langle M_mL_o|V|M_eL_o\rangle(E_e - E_m)^{-1} \quad (4a)$$

$$R_{om} = m_{mo}\mu_{om} = m_{mo}\mu_{oe}\langle M_eL_o|V|M_mL_o\rangle(E_m - E_e)^{-1} \quad (4b)$$

Two important points must be kept in mind in the analysis of a CD spectrum which arises by the one-electron mechanism. First, the potential operator V, expanded as a series of multipole functions, operates on the angular parts of wave functions. Therefore, symmetry reduces the operator to one term or at most to a small number of terms which give nonzero perturbation integrals for a given set of orbitals. For the chromophores in compounds **1** and **2**, which have D_{4h} symmetry, we need to consider, for example, the mixing of a magnetically accessible excited state transforming as $(R_x,R_y)(E_g)$ into an electronic excited state transforming as $(x,y)(E_u)$. To give finite mixing, the operator must transform as A_{1u}, the "pseudo-scalar" representation of D_{4h}. The lowest order multipole which transforms this way is a hexadecapole function, which has five nodal planes separating sectors of opposite sign. The parity properties of this function are shown in Figure 5. The physical meaning of this is that a perturbing point potential can give rise to positive, negative, or zero rotational strength, depending upon its location with respect to the chromophore. We cannot predict, a priori, the sign of a CD band arising under the one-electron mechanism. The signs of different transitions can, however, be related.

The second important point about rotational strengths is that for a given pair of excited states, $|M_mL_o\rangle$ and $|M_eL_o\rangle$, mixing in both directions gives rise to two CD bands of opposite sign. The denominators in eq 4a and 4b have opposite signs, while all other terms are the same in both equations. Thus, for one pair of excited states, $R_{oe} = -R_{om}$.

The CD transitions observed for compounds **1** and **2** arise from this one-electron mechanism. The relevant occupied and unoccupied molecular orbitals and transitions among them are summarized in Figure 6, which gives for each transition the symmetry of the operator (if any) under which the transition is allowed, as well as the energy difference in Hartrees between the orbitals in the ground state. The data in Figure 6 are from an Xα calculation[6] on $Rh_2(O_2CH)_4$.

For the CD transition at ~600 nm, the corresponding (x,y)-polarized electronic transition has been assigned as π^*(Rh–Rh) → σ^*(Rh–O), a promotion of an electron from the $5e_g$ level to $4b_{2u}$. As Figure 6 shows, the σ^*(Rh–O) manifold comprises two molecular orbitals; and promotion of an electron from π^*(Rh–Rh) to the second component of σ^*(Rh–O) ($5e_g \rightarrow 5b_{1g}$) is magnetically allowed. We assign the CD transition to π^*(Rh–Rh) → σ^*(Rh–O), which obtains rotational strength by mixing of the

D_{4h}		Rh-Rh σ* -0.1756 $4a_{2u}$	Rh-O σ* -0.1195 $4b_{2u}$	Rh-O σ* -0.1017 $5b_{1g}$	C-O π* -0.0105 $3b_{2g}$	C-O π* -0.0075 $7e_u$
Rh-Rh δ* -0.2208	$2b_{1u}$	0.0452 no basis	0.1013 R_z	0.1191 no basis	0.2103 z	0.2133 R_x,R_y
Rh-Rh π* -0.2343	$5e_g$	0.0587 x,y	0.1148* x,y	0.1326* R_x,R_y	0.2238 R_x,R_y	0.2268 z
Rh-Rh δ -0.2581	$2b_{2g}$	0.0825 no basis	0.1386 no basis	0.1564 R_z	0.2476 no basis	0.2506 x,y
Rh-Rh π Rh-O π -0.2632	$6e_u$	0.0876 R_x,R_y	0.1437* R_x,R_y	0.1615* x,y	0.2527 x,y	0.2557 R_z
O lone pair -0.2803	$1a_{1u}$	0.1047 R_z	0.1608 no basis	0.1786 no basis	0.2698 no basis	0.2728 R_x,R_y
O lone pair -0.2906	$4e_g$	0.1150 x,y	0.1711 x,y	0.1889 R_x,R_y	0.2801 R_x,R_y	0.2831 z
Rh-O σ Rh-Rh -0.3008	$5a_{1g}$	0.1252 z	0.1813 no basis	0.1991 no basis	0.2903 no basis	0.2933 x,y

Figure 6. Transition table for the molecular orbitals from the Xα calculation on $Rh_2(OOCH)_4$ (ref 6). MO's which are occupied in the ground state are shown at left, and MO's which are unoccupied in the ground state are at the top. Each box represents a possible transition, with the symmetry properties of the transition indicated along with the ground-state energy difference (in Hartrees) between the orbitals involved. Transitions marked with an asterisk are discussed in the text.

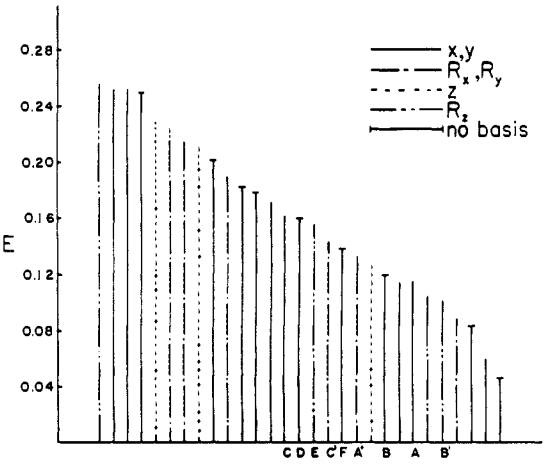

Figure 7. Diagrammatic representation of the possible electronic and magnetic transitions given in Figure 6. Ground-state energy differences between the orbitals involved in each transition are represented (in Hartrees) on the vertical axis. The transitions are laid out along the horizontal axis in decreasing order of the energy difference for each transition. The labeled transitions are the following: (A) $5e_g \rightarrow 4b_{2u}$, π^*(Rh–Rh) → σ^*(Rh–O); (A′) $5e_g \rightarrow 5b_{1g}$, π^*(Rh–Rh) → σ^*(Rh–O); (B) $2b_{1u} \rightarrow 5b_{1g}$, δ^*(Rh–Rh) → σ^*(Rh–O); (B′) $2b_{1u} \rightarrow 4b_{2u}$, δ^*(Rh–Rh) → σ^*(Rh–O); (C) $6e_u \rightarrow 5b_{1g}$, π(Rh–Rh,Rh–O) → σ^*(Rh–O); (C′) $6e_u$ → $4b_{2u}$, π(Rh–Rh, Rh–O) → σ^*(Rh–O); (D) $1a_{1u} \rightarrow 4b_{2u}$, O lone pair → σ^*(Rh–O); (E) $2b_{2g} \rightarrow 5b_{1g}$, δ(Rh–Rh) → σ^*(Rh–O); (F) $2b_{2g} \rightarrow 4b_{2u}$, δ(Rh–Rh) → σ^*(Rh–O).

magnetic excited state (with an electron in $5b_{1g}$) into the electronic excited state (with an electron in $4b_{2u}$). With the mixing in this direction, the CD band appears at the same energy as the electronic transition.

Our data do not directly address the question of the identity of the 297-cm^{-1} vibrational band. However, our assignment of the 600-nm CD peak lends support to the assignment of the vibrational band as the symmetrical Rh–O(carboxylate) stretch.

We assign the CD band at ~450 nm in an analogous way. The electronic transition has been assigned as π(Rh–Rh,Rh–O) → σ^*(Rh–O). The promotion of an electron from the π-level ($6e_u$) to one component of σ^*(Rh–O) ($5b_{1g}$) is allowed with the observed (x,y)-polarization. The promotion $6e_u \rightarrow 4b_{2u}$ is magnetically allowed, and the CD band results from perturbation mixing of the magnetically accessible excited state, with an electron in $4b_{2u}$,

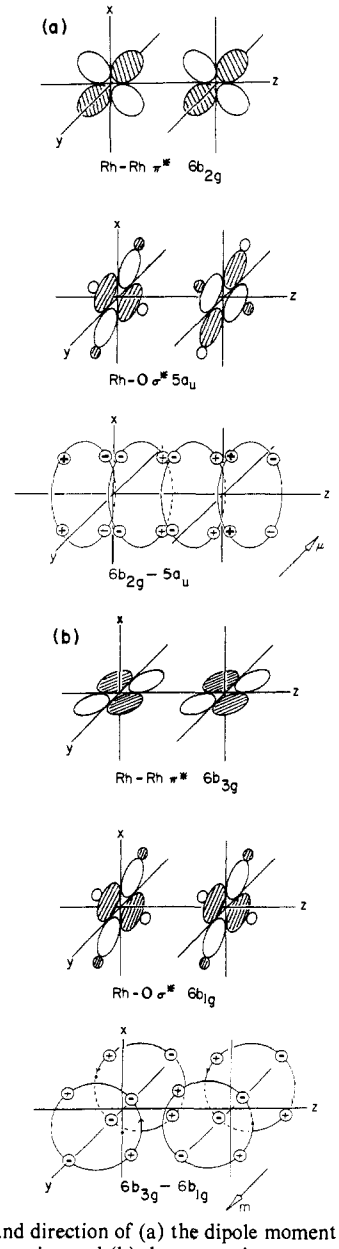

Figure 8. Origin and direction of (a) the dipole moment associated with the $6b_{2g} \rightarrow 5a_u$ promotion and (b) the magnetic moment associated with promoting an electron from $6b_{3g} \rightarrow 6b_{1g}$ in the π^*(Rh–Rh) $\rightarrow$ σ^*(Rh–O) transitions of dirhodium tetracarboxylates. See the text for a full discussion.

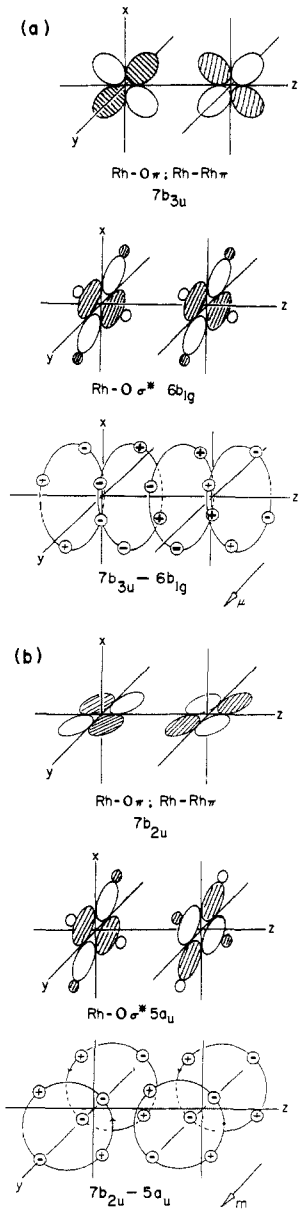

Figure 9. Origin and direction of (a) the dipole moment associated with the $7b_{3u} \rightarrow 6b_{1g}$ electronically allowed transition and (b) the magnetic moment associated with the magnetically allowed promotion $7b_{2u} \rightarrow 5a_u$ in the π(Rh–Rh, Rh–O) $\rightarrow$ σ^*(Rh–O) transition envelope of the singly bonded dirhodium tetracarboxylates. See the text for a full discussion.

into the electronic excited state, in which $5b_{1g}$ is populated.

The mixing scheme for these assignments is shown diagrammatically in Figure 7. In the figure, the energy differences shown are those between ground-state orbitals. The excited state arising from magnetic transition A′ ($5e_g \rightarrow 5b_{1g}$) is mixed into that arising from electronic transition A ($5e_g \rightarrow 4b_{2u}$), giving rise to the CD band at ~600 nm. Mixing of the excited state resulting from magnetic transition C′ ($6e_u \rightarrow 4b_{2u}$) into that from electronic transition C ($6e_u \rightarrow 5b_{1g}$) gives rise to the CD band at ~450 nm.

(b) Relative Signs of the CD Bands Near 600 and 450 nm. We are able to show why the CD transitions at 600 and 450 nm have the same sign for a given compound, based on our assignments of the bands. In order to do this, we consider the relative directions of the electric and magnetic moments corresponding to each transition. We conduct this analysis for the molecular orbitals under point group D_{2h}, in which we avoid the complications caused by two-dimensional symmetry representations without losing any physical validity. (The levels are from an Xα calculation[6] on $Rh_2(O_2CH)_4(H_2O)_2$.) Figure 8a shows the orbitals involved in the electronically allowed component of the π^*(Rh–Rh) $\rightarrow$ σ^*-(Rh–O) transition ($6b_{2g} \rightarrow 5a_u$ in D_{2h}). The direction of the dipole moment is determined by the charge distribution in the product function of the two orbitals.[14] Wherever the product function is positive, electrons are present and the relative charge is negative. The resulting multipole charge distribution is shown at the bottom of Figure 8a. Overlap in the area between the metal centers leads to diminution of the charges, and so for this transition the charge distribution outside the area between the metal atoms is dominant. Thus, the resulting dipole moment for this transition is in the negative y-direction. For the magnetically allowed π^*(Rh–Rh) $\rightarrow$ σ^*(Rh–O) transition ($6b_{3g} \rightarrow 6b_{1g}$), shown in Figure 8b, the promotion of the electron involves a counterclockwise rotation about the positive y-axis. Thus, the magnetic moment associated with this transition is in the positive y-direction. We note here that, although the two moments associated with this transition are in opposite directions, the absolute sign of the resulting CD peak is not yet determined; it still depends upon the sign of the potential which mixes the two excited states.

For the 450-nm CD band, the development of the moments for the two transitions involved is shown in Figure 9. For the electronically allowed transition ($7b_{3u} \rightarrow 6b_{1g}$, Figure 9a), the charge distribution in the product function is augmented in the

region between the metal atoms, by overlap between the two metals. The resulting dipole moment is along the positive y-axis. The magnetically allowed transition ($7b_{2u} \rightarrow 5a_u$, Figure 9b) involves a counterclockwise charge rotation about the y-axis and a consequent dipole moment along positive y.

For the 600-nm CD transition, the electric and magnetic moments are in opposite directions, while for the 450-nm band the two moments are parallel. Although the relationships of electric and magnetic moments are counterposed for the two bands, so also are the perturbation coefficients for excited-state mixing in the two cases. The denominator in eq 4a is different in sign for the two transitions in the absence of a very unlikely, major rearrangement of lower lying energy levels upon activation of any of the transitions under consideration. We can see from Figure 7 that the 600-nm CD band arises from mixing of a higher energy magnetic excited state into a lower lying electronic excited state. The denominator in eq 4a for this transition is, therefore, negative. As Figure 7 shows, the opposite is true for the 450-nm CD band.

With our assignments of the CD bands, then, the bands at 600 and 450 nm *must* have the same sign. We observe this for both compounds **1** and **2**, and we have observed the same effect in some half-dozen other chiral compounds with the same $Rh_2(O_{eq})_8(O_{ax})_2$ chromophore (to be reported elsewhere). This gives further support to the assignments as well as to the applicability of the one-electron, static-coupling mechanism to these compounds.

(c) Assignment of the CD Band at 500 nm. We have already discussed the fact that mixing of a magnetically accessible excited state into an electronically accessible state can be accompanied by a reverse mixing which gives rise to a CD effect with a sign opposite to that of the first. In compounds **1** and **2** we observe, in the area between the 600- and 450-nm bands, a third CD effect, opposite in sign to the first two. As Figure 7 shows, the relevant magnetic transitions are near each other in the region between the electronic transitions. We assign the 500-nm band to an overlap of these two magnetically allowed transitions, which are activated in the CD by the reverse-mixing process. There is no question about the nature of the 500-nm band; it does not appear in the electronic spectrum, and, therefore, it is a magnetically allowed transition.

While there is little doubt that the assigned transitions are active in this region, it is also possible that a magnetically allowed $\delta(Rh-Rh) \rightarrow \sigma^*(Rh-O)$ transition is also active (transition E in Figure 7). This could affect the relative intensities of the three CD peaks; we are currently investigating this and other features of the CD spectra of chiral dirhodium tetracarboxylates.

Acknowledgment. We are grateful to the National Science Foundation for support. We also thank Professor Graham Palmer of Rice University for very graciously allowing us to use his JASCO (J500-C) CD/ORD spectrometer to check and confirm our observations.

Registry No. 1, 100019-76-9; **2**, 100019-77-0.

Supplementary Material Available: Full tables of bond distances and angles, anisotropic displacement parameters, and observed and calculated structure factors for the crystal structures of **1** and **2** (91 pages). See any current masthead page for ordering information.

High-Valent Iron Porphyrins: Synthesis, X-ray Structures, π-Cation Radical Formulation, and Notable Magnetic Properties of Chloro(*meso*-tetraphenylporphinato)iron(III) Hexachloroantimonate and Bis(perchlorato)(*meso*-tetraphenylporphinato)iron(III)

Pierre Gans,[1] Georges Buisson,[2] Emile Duée,[2] Jean-Claude Marchon,*[1] Brian S. Erler,[3] William F. Scholz,[3] and Christopher A. Reed*[3]

Contribution from the Département de Recherche Fondamentale, Centre d'Études Nucléaires de Grenoble, 85X, 38041 Grenoble, France, and Department of Chemistry, University of Southern California, Los Angeles, California 90089-1062. *Received July 22, 1985*

Abstract: The collective evidence from electronic, infrared, Mössbauer, and ^1H NMR spectroscopies, from X-ray crystal structure determinations, from electrochemical studies, and from magnetic susceptibility data provides unambiguous evidence that $[FeCl(TPP\cdot)]^+$ and $Fe(OClO_3)_2(TPP\cdot)$ (TPP = *meso*-tetraphenylporphinate) are iron(III) porphyrin π-cation radical species rather than iron(IV) complexes. The distinction is real, not semantic, and greatly affects the physical and chemical properties of high-valent iron porphyrins. Strong antiferromagnetic coupling ($|-2J| \gtrsim 500$ cm^{-1}) of the $S = {}^5/_2$ iron atom with the $S = {}^1/_2$ porphyrin radical leads to an overall $S = 2$ state for $[FeCl(TPP\cdot)][SbCl_6]$ (**1**) ($\mu_{eff}^{300K} = 4.8\ \mu_B$). By contrast, ferromagnetic coupling ($2J \simeq +80$ cm^{-1}) in $Fe(OClO_3)_2(TPP\cdot)$ (**2**) leads to an $S = 3$ ground state ($\mu_{eff}^{300K} = 6.5\ \mu_B$). X-ray crystal structure determinations of the *p*-tolyl analogue of **1**, $[FeCl(TpTP\cdot)][SbCl_6]\cdot 2C_2H_2Cl_4$ (**3**), and of **2** provide an orbital symmetry rationale for this sharply contrasting magnetic behavior and give new insight into the magnetic coupling of a metal to a porphyrin cation radical. An explanation is offered for the insignificant coupling ($J \sim -2$ cm^{-1}) in compound I of horseradish peroxidase. Crystal data for **3**: monoclinic, space group $P2_1/c$, $Z = 4$, $a = 10.98$ (1) Å, $b = 22.57$ (1) Å, $c = 23.65$ (1) Å, $\beta = 97.73$ (5)° at −140 °C, $R = 0.088$, $R_w = 0.097$, Fe–N_{av} = 2.07 (1) Å, Fe–Cl = 2.168 (5) Å. Crystal data for **2**: monoclinic, space group $P2_1/c$, $Z = 2$, $a = 12.132$ (1) Å, $b = 14.622$ (2) Å, $c = 13.153$ (1) Å, $\beta = 127.84$ (1)° at 25 °C, $R = 0.116$, $R_w = 0.130$, Fe–N_{av} = 2.045 (10) Å, Fe–O = 2.13 (1) Å.

High-valent iron porphyrin complexes have been challenging target molecules for synthetic inorganic chemists during the last decade. The term "high-valent" is used to refer to iron porphyrin complexes more oxidized than the iron(III) oxidation state, the stable state under aerobic conditions. The intense interest in these compounds stems from the demonstrated or proposed involvement of species of this type in various biological processes mediated by peroxidase and catalase,[4-6] by cytochrome P-450,[7] and in model

(1) Laboratoires de Chimie, Département de Recherche Fondamentale.
(2) Service de Physique, Département de Recherche Fondamentale.
(3) University of Southern California.

0002-7863/86/1508-1223$01.50/0